

Non-destructive study of non-equilibrium states of cold, trapped atoms

Maria Brzozowska, Tomasz M. Brzozowski, Jerzy Zachorowski, and Wojciech Gawlik*
Marian Smoluchowski Institute of Physics, Jagiellonian University, Reymonta 4, PL 30-059 Cracow†
(Dated: 9th February 2020)

We report on the non-destructive, real-time spectroscopic determination of the 2D kinetic momentum distribution of a cold-atom sample. The method is based on the three-beam measurement of the recoil-induced resonances. It can be applied for atoms in a working trap, i.e. constantly perturbed by the trap fields, and yields the real-time, in-situ diagnostics of the 2D atomic momentum distribution. The method is versatile, accurate and works in a wide range of trapping parameters. We used it to demonstrate various non-equilibrium states of atoms in an operating magneto-optical trap. In particular, we demonstrated anisotropy of the momentum distribution of atomic sample in the trap with unequal intensities of the trapping beams.

PACS numbers: 32.80.Pj, 42.50.Vk, 42.65.-k

In experiments with cold, dilute atomic gases, the first cooling stage usually employs a magneto-optical trap (MOT), which yields temperatures in a range of hundreds to a few μK . Further traps and cooling stages can be applied for reaching the quantum degeneracy regime. This requires matching of the momentum distributions of various traps. Knowledge of such distributions is also essential for quantum state diagnostics of the trapped sample. Below, we present reliable 2D diagnostics method based on the so called recoil-induced resonances (RIRs) and apply it to study non-standard momentum distributions in a MOT.

The RIRs result from a stimulated Raman process, which couples two kinetic states of free moving atoms (Fig. 1). The coupling is accomplished by interaction with two laser beams, the pump and the probe, of frequencies ω and $\omega + \delta$, respectively. As a result of the Raman transition, the atoms gain kinetic energy $\Delta E_{\text{kin}} = \hbar\delta$ and change momentum \mathbf{p} by $\Delta\mathbf{p} = \hbar\Delta\mathbf{k} = \pm 2\hbar k \hat{\mathbf{e}}_i \sin \theta/2$, where k is the modulus of the light wave vector, θ is the angle between the beams, and $\hat{\mathbf{e}}_i$ is the unit vector perpendicular to the bisector of θ . The sign in $\Delta\mathbf{p}$ depends on the direction of the Raman process. The non-zero amplitude of the considered Raman resonance arises from different populations of the given kinetic states. When recorded in absorption, the RIR shape is proportional to a derivative of the momentum distribution $\partial\Pi(p_i)/\partial p_i$, where $p_i = \mathbf{p} \cdot \hat{\mathbf{e}}_i$ [1, 2, 3, 4, 5, 6]. This direct relation of the RIR signal to $\Pi(\mathbf{p})$ allows convenient and accurate measurement of the kinetic momentum distribution in a cold atomic sample, provided that the distribution is sufficiently narrow.

The first unambiguous observation of RIRs was made in a 1D optical lattice [1] filled with atoms much colder than in a standard MOT. RIR signals were also seen in optical molasses [7, 8], in a cold atomic beam [9] and with atoms released from a MOT [10]. The significance

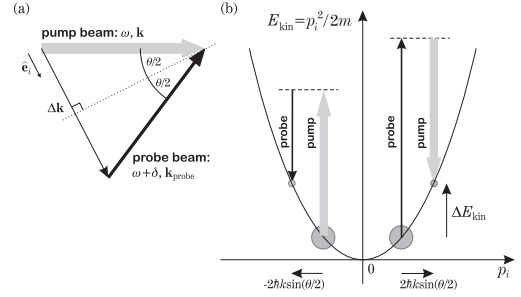


Figure 1: Recoil-induced resonances: (a) Geometry of the laser beams, (b) the atomic kinetic energy and momentum changes due to the Raman process coupling two kinetic states. Circles symbolize populations $\Pi(\mathbf{p})$ of these states.

of the recoil effect in a continuously working MOT and its influence on the probe absorption and four wave mixing spectra has been recently demonstrated in Ref. [3].

The big advantage of the RIR method is its directional selectivity. $\Pi(\mathbf{p})$ is probed in a given direction, specified by the angle between the probe and the pump beams (Fig.1a). Hence, apart from applications to standard 1D velocimetry [7, 9], RIRs can also be used for studies of a possible momentum distribution anisotropy in non-equilibrium states of a cold atomic sample. For example, atoms in a MOT can be driven away from thermal equilibrium by introducing appropriate asymmetry in the trapping parameters. In particular, as predicted in Ref. [11] and demonstrated below, when the trapping light intensity in a MOT is unevenly distributed between the trapping beams, the width of $\Pi(\mathbf{p})$ becomes direction-dependent.

In this Letter we present evidence of three different kinds of anisotropy of the momentum distribution in a constantly operating MOT, i.e. with all light and magnetic fields on. The measurement was conducted using our three-beam, RIR-based method for simultaneous probing of the momentum distribution in two perpendicular directions. The method extends the principle of 1D thermometry as suggested by Meacher et al. [7]. Important feature of our extension is that 2D information is

*Electronic address: gawlik@uj.edu.pl

†URL: <http://www.if.uj.edu.pl/ZF/qnog/>

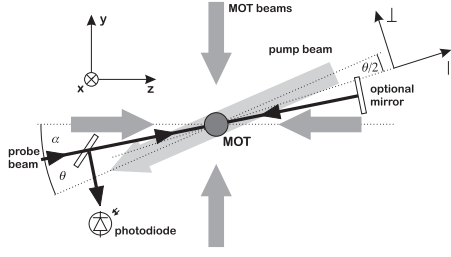


Figure 2: The layout of the experiment. The pump and probe beams intersect in a cloud of cold atoms in the working MOT. With the optional mirror we realize a three-beam configuration in which the momentum exchange is allowed in two directions: \perp and \parallel . Third pair of the MOT beams along x and the MOT coils are not shown in this figure.

acquired simultaneously in one measurement.

In our experiment (Fig. 2) the ^{85}Rb atoms are trapped and cooled in a standard vapor-loaded MOT [12]. Additionally, two beams intersecting in the trap center are introduced: the pump and the probe. The probe beam is directed at a small angle $\alpha = 3^\circ$ to the MOT beams (propagating along z), and the pump is at $\theta = 5^\circ$ to the probe. The probe beam can be detected either directly or after retroreflection. The setup with retroreflected probe enables the measurement of $\Pi(\mathbf{p})$ simultaneously along two perpendicular directions: \perp , for angle θ between the pump and the nearly co-propagating probe, and \parallel , for angle $180^\circ - \theta$ between the pump and the nearly counter-propagating probe. When α and θ are sufficiently small, \perp and \parallel almost coincide with the y and z directions, respectively. Both pump and probe beams are derived from diode lasers synchronized by injection-locking and are blue-detuned from the trapping transition $^2\text{S}_{1/2}(F=3) \rightarrow ^2\text{P}_{3/2}(F'=4)$ by $\Delta = 2\pi \cdot 140 \text{ MHz} \approx 23.3\Gamma$, where Γ denotes the natural linewidth. Detuning of this size reduces the atomic perturbation to a very low level (scattering rate $\propto 1/\Delta^2$) which is essential for non-destructive measurements. Despite large Δ , the pump and probe beams drive the Raman signal with a sufficiently large amplitude and signal-to-noise ratio for the pump beam intensities $5\text{--}35 \text{ mW/cm}^2$. In principle, one could retroreflect the pump- rather than probe-beam. Such solution, however, would introduce extra complications due to the standing-wave pattern of a strong pump.

The probe beam is scanned by $\delta \approx \pm 1 \text{ MHz}$ around frequency ω of the pump beam. The probe and pump photons induce Raman transitions between the atomic kinetic states separated by $\pm \hbar\delta$. Since the polarization of the pump and probe beams is chosen to be the same, the atoms undergo Raman transitions with $\Delta m_F = 0$. Hence, the internal atomic state does not change and the only states that have to be considered are the external states associated with the kinetic energy of the atomic center-of-mass. The multi-level structure of ^{85}Rb can thus be reduced to a set of independent two-level transitions which allows straightforward application of the basic RIR theory [1, 2]. With the assumption that

$\Pi(\mathbf{p})$ is the Maxwell-Boltzmann distribution, the RIR signal $s(\delta)$ [2, 3] recorded with the retroreflected probe is given by two contributions. The first one results from the Raman process involving the pump and the probe beam making small angle θ and the wide one is for angle $180^\circ - \theta$. The signal is

$$s(\delta) \propto -A_{\perp} \delta \exp\left(-\frac{\delta^2}{\xi_{\perp}^2}\right) - A_{\parallel} \delta \exp\left(-\frac{(\delta - \delta_0)^2}{\xi_{\parallel}^2}\right), \quad (1)$$

where, for small θ , $\xi_{\perp}^2 \approx 2k_B k^2 m^{-1} \theta^2 \tau_{\perp}$ and $\xi_{\parallel}^2 \approx 8k_B k^2 m^{-1} \tau_{\parallel}$. τ_{\perp} and τ_{\parallel} are the distribution widths in the \perp and \parallel directions in the temperature units, A_{\parallel} and A_{\perp} are the amplitudes of the corresponding contributions, m is the atomic mass and k_B is the Boltzmann constant, and δ_0 is the possible frequency shift between the \perp and \parallel contributions, to be discussed later.

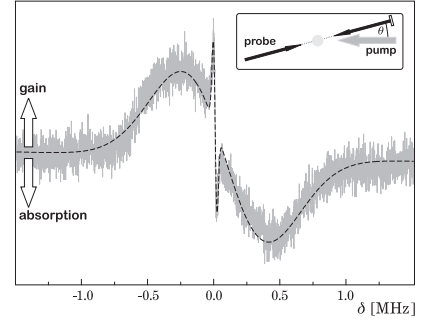


Figure 3: Transmission spectrum of a retroreflected probe (gray) and the theoretical prediction (dashed) of eq.(1). The beam setup is shown in the inset. The MOT beams have intensity $I_{\text{MOT}} = 13.8 \text{ mW/cm}^2$ per beam and are detuned from the trapping transition by $\Delta_{\text{MOT}} = -3\Gamma$, the repumper beam intensity $I_{\text{REP}} = 15 \text{ mW/cm}^2$, the axial magnetic field gradient $\partial_x B = 12 \text{ Gauss/cm}$, the pump beam intensity $I = 33 \text{ mW/cm}^2$, the probe beam total power $P \approx 2 \mu\text{W}$ and diameter $\sigma = 1 \text{ mm}$.

Typical example of the retroreflected-probe transmission spectrum is shown in Fig. 3. It exhibits two distinct resonant contributions, as predicted by eq. (1). The wide contribution is shifted with respect to the narrow one by 72.4 kHz , which indicates a non-zero average momentum component in the \parallel direction [19]. This is evidence of a slow (2.8 cm/s) atomic drift resulting from a small imbalance of the radiation pressures intrinsic to a MOT with retroreflected trapping beams. It has been checked that this shift increases when the imbalance is purposely increased. As the velocity distributions derived from the signal in Fig. 3 are Gaussian, one can determine the values $\tau_{\perp} = 171.7 \pm 6.2 \mu\text{K}$ and $\tau_{\parallel} = 170.1 \pm 3.2 \mu\text{K}$. The equality of these τ s implies thermodynamical equilibrium and allows their interpretation as temperature T . The equilibrium is due to the fact that total intensities of each pair of the beams remain the same and persists for various MOT-beams intensities (Fig. 4). The quasi-linear

increase of T with the total MOT-beams intensity agrees well with previous observations [15, 16, 17].

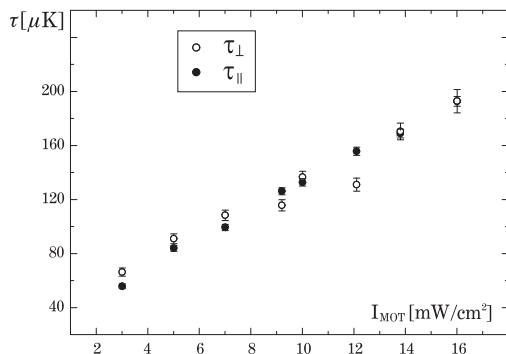


Figure 4: Trapped atoms in a thermal equilibrium: the dependence of widths τ_{\perp} and τ_{\parallel} on the intensity of the MOT beams (the intensity is given per one MOT beam). Other parameters are the same as in the case of Fig. 3.

The thermodynamics of the system becomes different when the trapping light is unevenly distributed between the MOT beam pairs.

For such conditions, Gajda and Mostowski predicted in Ref. [11] that the width of kinetic momentum distribution becomes direction-dependent. Such anisotropy is a signature of the non-equilibrium state of the cold atom cloud. Exploiting the simultaneous measurement of the momentum width in two perpendicular directions, we verified whether such an anisotropy in a MOT can be observed. For this reason, we changed intensity balance between the longitudinal (I_z) and transverse (I_x, I_y) MOT beam pairs, while keeping the total intensity $I_0 = I_x + I_y + I_z$ constant. We define parameter κ as the relative intensity of I_z , $I_z = \kappa I_0$, $I_x = I_y = (1 - \kappa)I_0/2$. The results of the measurement of τ_{\parallel} and τ_{\perp} for different values of κ are depicted in Fig 5. For equal partition of the trapping intensity ($\kappa = 1/3$), the widths of kinetic momentum distributions are the same as expected. However, when κ increases, τ_{\parallel} and τ_{\perp} follow opposite trends, which is evidence of kinetic momentum anisotropy in a working MOT and thereby its non-equilibrium state. We notice that $\tau_{\parallel} + 2\tau_{\perp}$ which is the measure of $v_{\parallel}^2 + 2v_{\perp}^2$ is constant within $\pm 2\%$ over the whole measured range of κ shown in Fig. 5. The decrease of τ_{\parallel} with the growing κ is due to the fact that the heating associated with spontaneous emission is isotropic, whereas the cooling rate is higher for the direction with the increased intensity. The momentum anisotropy becomes manifest because the density of the atoms is too small to provide efficient thermalization. Simple estimation for typical conditions and Rb-Rb collision cross-section $\sigma_{\text{Rb-Rb}} = 3 \cdot 10^{-13} \text{ cm}^2$ yields the atomic collision rate below 1 Hz in our trap, while the friction coefficient, in frequency units, is in the kHz range.

The theoretical behavior of τ_{\parallel} and τ_{\perp} according to the formulas from Refs. [11, 13] is plotted in Fig. 5 along with the experimental data. They exhibit similar qualitative behavior (the decrease of τ_{\parallel} and the increase

of τ_{\perp} with growing κ), but the theory fails to reproduce the exact shape of the experimental dependence. We attribute this discrepancy to additional mechanism of sub-Doppler cooling involving multilevel structure of ^{85}Rb atoms, which is not included in the calculations of Ref. [11]. The increase of I_z accompanied by attenuation of I_x and I_y results in a very efficient quasi-1D cooling scheme in the $\sigma^+ - \sigma^-$ optical molasses [14]. Evidence of this cooling is provided by the values of τ_{\parallel} falling to $70 \mu\text{K}$, well below the Doppler cooling limit of $140 \mu\text{K}$.

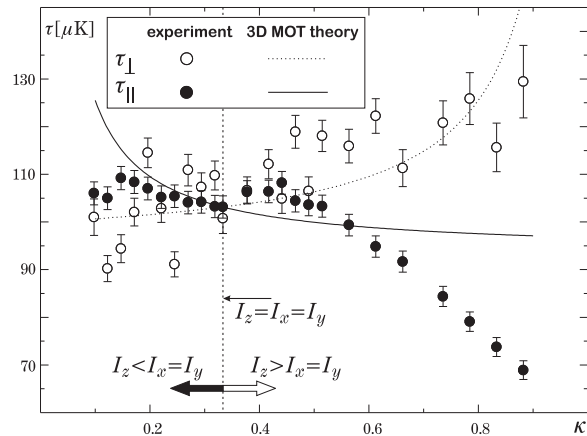


Figure 5: The measured widths of the kinetic momentum distributions in the two perpendicular directions, τ_{\perp} (hollow circles) and τ_{\parallel} (filled circles), as a function of relative intensity κ . For the equilibrium ($\kappa = 1/3$), $I_{\text{MOT}} = 6.8 \text{ mW/cm}^2$, $\tau_{\perp} = 100 \pm 3 \mu\text{K}$ and $\tau_{\parallel} = 103 \pm 2 \mu\text{K}$. Other parameters as in Fig. 3. Theoretical curves are plotted according to Refs. [11, 13].

In the situation discussed above, the MOT beams were carefully aligned which resulted in high stability of the trapped-atom cloud, even for the largest departures from the equal partition of the trapping light intensity, and allowed fitting of the RIR signals by expression (1). The sole manifestation of the non-equilibrium state of the sample was the anisotropy of $\Pi(\mathbf{p})$.

The thermodynamics equilibrium can be altered yet in a different way, namely by enhancing imbalance between the counter-propagating MOT-beam radiation pressures. Fig. 6a depicts the RIR recorded with a standard 1D, two-beam arrangement applied to the case when the MOT beams were slightly misaligned and detuned closer to resonance. The 1D thermometry was accomplished by replacing the optional mirror in (Fig. 2) by a photodiode. In this configuration, the pump and the probe beams form the angle $180^\circ - \theta$ and the recorded signal is proportional only to $\partial \Pi(p_{\parallel}) / \partial p_{\parallel}$. Its shape deviates from a derivative of a Gaussian curve. It is straightforward to obtain the actual distribution of velocity component in the \parallel direction, v_{\parallel} , by integrating the probe transmission signal and scaling to the velocity units: for small θ , $v_{\parallel} \approx \delta/2k$. To emphasize the departure of the actual velocity distribution from the case of the thermal equilibrium, the distribution obtained from experimen-

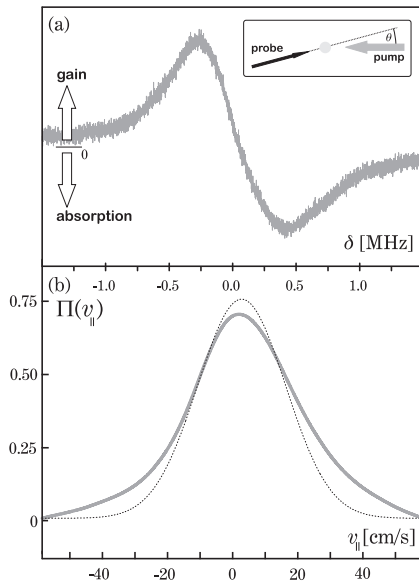


Figure 6: (a) The probe transmission spectrum in a misaligned MOT for $I_{\text{MOT}} = 3.1 \text{ mW/cm}^2$, $\Delta_{\text{MOT}} = -2.25\Gamma$ and other experimental parameters as in Fig 3. As shown in inset, the probe-beam is not retroreflected, hence only the wide RIR contribution is present. (b) The actual velocity distribution $\Pi(v_{||})$ (grey thick line) obtained by integrating the probe transmission spectrum and the Gaussian reference (dotted line), defined in text.

tal signal is shown in Fig. 6b together with the idealized Gaussian curve of the same area and of the width derived from the positions of the minimum and maximum of the RIR signal in Fig. 6a.

In conclusion, we have worked out three-beam spectroscopic method of determining the momentum distri-

butions of cold, trapped atoms, based on recoil-induced resonances. Its potential has been demonstrated by study of three different momentum distributions of atoms in the operating magneto-optical trap: (i) thermodynamic equilibrium with well defined temperature and Gaussian momentum distribution with a slow velocity drift; (ii) non-equilibrium state characterized by Gaussian distributions with drastically different widths in the longitudinal and transverse directions; (iii) non-equilibrium state of asymmetric momentum distribution along one direction. The result (ii) qualitatively confirms theoretical predictions of Ref. [11] and indicate need for more detailed theory. Our method allows accurate determination of the momentum distributions simultaneously in two perpendicular directions and can be straightforwardly applied to 3D case. It can be used for the non-destructive, on-line diagnostics of the atom dynamics in a trap and carried out independently and simultaneously with the other spectroscopic measurements. The method should also be applicable to quantum-degenerate gases. In fact, the widely used Bragg spectroscopy is based on the same principle of momentum and energy transfer: it measures the momentum gained by atoms whereas RIR measures the complementary photonic loss. Measuring the Bragg-beam transmission in our three-beam geometry, rather than imaging the BEC shape can become a valuable, non-destructive alternative to standard diagnostics of ultra-cold, trapped atoms.

This work was supported by the Polish Ministry of Science and Information Society Technologies and is part of a general program on cold-atom physics of the National Laboratory of AMO Physics in Toruń, Poland. Authors would like to thank Mariusz Gajda for his illuminating discussion [13] and Krzysztof Sacha for his valuable comments.

-
- [1] G. Grynberg, J.-Y. Courtois, B. Lounis, and P. Verkerk, Phys. Rev. Lett. **72**, 3017 (1994).
 - [2] P. Verkerk, Proceedings of The International School of Physics, Varenna, **Course CXXXI**, 325 (1996).
 - [3] T. M. Brzozowski, M. Brzozowska, J. Zachorowski, M. Zawada, and W. Gawlik, Phys. Rev. A **71**, 013401 (2005).
 - [4] J. Guo, P. R. Berman, B. Dubetsky, and G. Grynberg, Phys. Rev. A **46**, 1426 (1992).
 - [5] J. Guo and P. R. Berman, Phys. Rev. A **47**, 4128 (1993).
 - [6] B. Dubetsky and P. R. Berman, Phys. Rev. A **52**, R2519 (1995).
 - [7] D. R. Meacher, D. Boiron, H. Metcalf, C. Salomon, and G. Grynberg, Phys. Rev. A **50**, R1992 (1994).
 - [8] M. C. Fischer, A. M. Dudarev, B. Gutiérrez-Medina, and M. G. Raizen, J. Opt. B: Quantum Semiclass. Opt. **3**, 279 (2001).
 - [9] G. Di Domenico, G. Miletì and P. Thomann, Phys. Rev. A **64**, 043408-1 (2001).
 - [10] Y.-C. Chen, Y.-W. Chen, J.-J. Su, J.-Y. Huang, and I. A. Yu, Phys. Rev. A **63**, 043808 (2001).
 - [11] M. Gajda and J. Mostowski, Phys. Rev. A **49**, 4864 (1994).
 - [12] E. L. Raab, M. Prentiss, A. Cable, S. Chu, and D. E. Pritchard, Phys. Rev. Lett. **59**, 2631 (1987).
 - [13] M. Gajda, *private communication*.
 - [14] J. Dalibard and C. Cohen-Tannoudji, J. Opt. Soc. Am. B **6**, 2023 (1998).
 - [15] P. D. Lett, W. D. Phillips, S. L. Rolston, C. E. Tanner, R. N. Watts, C. I. Westbrook, J. Opt. Soc. Am. B **6**, 2085 (1989).
 - [16] C. D. Wallace, T. P. Dinneen, K. Y. N. Tan, A. Kumarakrishnan, P. L. Gould and J. Javanainen, J. Opt. Soc. Am. B, **11**, 703 (1994).
 - [17] X. Xu, T. H. Loftus, M. J. Smith, J. L. Hall and A. Gallagher and J. Ye, Phys. Rev. A **66**, 011401(R) (2002).
 - [18] U. D. Rapol and A. Wasan and V. Natarajan, Phys. Rev. A, **46**, 023402 (2001).
 - [19] The possible drift in the perpendicular direction cannot be detected in this setup as the shifts of the two resonances are proportional to their widths.